



**HAL**  
open science

## Alignment control and atomically-scaled heteroepitaxial interface study of GaN nanowires

Qingyun Liu, Baodan Liu, Wenjing Yang, Bing Yang, Xinglai Zhang,  
Christophe Labbe, Xavier Portier, Vladimir An, Xin Jiang

► **To cite this version:**

Qingyun Liu, Baodan Liu, Wenjing Yang, Bing Yang, Xinglai Zhang, et al.. Alignment control and atomically-scaled heteroepitaxial interface study of GaN nanowires . *Nanoscale*, 2017, 9, pp.5212-5221. 10.1039/C7NR00032D . hal-01507361

**HAL Id: hal-01507361**

**<https://hal.science/hal-01507361v1>**

Submitted on 28 Apr 2017

**HAL** is a multi-disciplinary open access archive for the deposit and dissemination of scientific research documents, whether they are published or not. The documents may come from teaching and research institutions in France or abroad, or from public or private research centers.

L'archive ouverte pluridisciplinaire **HAL**, est destinée au dépôt et à la diffusion de documents scientifiques de niveau recherche, publiés ou non, émanant des établissements d'enseignement et de recherche français ou étrangers, des laboratoires publics ou privés.

# Alignment control and atomically-scaled heteroepitaxial interface study of GaN nanowires†

Qingyun Liu,<sup>a,b</sup> Baodan Liu,<sup>a</sup> \*<sup>a</sup> Wenjin Yang,<sup>a</sup> Bing Yang,<sup>a</sup> Xinglai Zhang,<sup>a</sup> Christophe Labbé,<sup>c</sup> Xavier Portier,<sup>c</sup> Vladimir An<sup>d</sup> and Xin Jiang<sup>\*a</sup>

Well-aligned GaN nanowires are promising candidates for building high-performance optoelectronic nanodevices. In this work, we demonstrate the epitaxial growth of well-aligned GaN nanowires on a [0001]-oriented sapphire substrate in a simple catalyst-assisted chemical vapor deposition process and their alignment control. It is found that the ammonia flux plays a key role in dominating the initial nucleation of GaN nanocrystals and their orientation. Typically, significant improvement of the GaN nanowire alignment can be realized at a low NH<sub>3</sub> flow rate. X-ray diffraction and cross-sectional scanning electron microscopy studies further verified the preferential orientation of GaN nanowires along the [0001] direction. The growth mechanism of GaN nanowire arrays is also well studied based on cross-sectional high-resolution transmission electron microscopy (HRTEM) characterization and it is observed that GaN nanowires have good epitaxial growth on the sapphire substrate following the crystallographic relationship between (0001)<sub>GaN</sub>|| (0001)<sub>sapphire</sub> and (10 $\bar{1}$ 0)<sub>GaN</sub>|| (11 $\bar{2}$ 0)<sub>sapphire</sub>. Most importantly, periodic misfit dislocations are also experimentally observed in the interface region due to the large lattice mismatch between the GaN nanowire and the sapphire substrate, and the formation of such dislocations will favor the release of structural strain in GaN nanowires. HRTEM analysis also finds the existence of "type I" stacking faults and voids inside the GaN nanowires. Optical investigation suggests that the GaN nanowire arrays have strong emission in the UV range, suggesting their crystalline nature and chemical purity. The achievement of aligned GaN nanowires will further promote the wide applications of GaN nanostructures toward diverse high-performance optoelectronic nanodevices including nano-LEDs, photovoltaic cells, photodetectors etc.

## Introduction

Semiconductor nanostructures with crystalline quality and good alignment have been extensively explored as ideal building blocks for various nanoscale electronic and photonic applications.<sup>1-3</sup> The nanostructure geometry with advantages of a large surface-to-volume ratio and low dimensions shows intriguing optoelectronic properties superior to their

thin-film and bulk counterparts. The representative examples of nanostructure applications, such as high efficiency solar cells made from ordered arrays of silicon nanowires,<sup>4</sup> high performance photoelectrodes constructed from p-type silicon wire-arrays<sup>5</sup> or 3D ordered Au/B-ZnO nanowires<sup>6</sup> for solar energy conversion and the hierarchical assembly of one-dimensional nanostructures into well-defined functional networks,<sup>7</sup> are often reported in the literatures. Particularly, crystalline GaN nanostructures in the forms of nanowires, nanotubes and nanorods are employed in the context of specific applications such as field-emission transistors (FETs), nano-lasers, light-emitting diodes (LEDs) and overall water splitting photocatalysts due to their high electron mobility, tunable direct band-gap and excellent photoelectric sensitivity.<sup>8-15</sup> For GaN crystals, two polymorphs like thermodynamically favorable wurtzite and metastable zinc-blende type structures are generally observed. The wurtzite GaN has an anisotropic crystal structure, and many of its properties are closely dependent upon the crystal orientation.<sup>16,17</sup> In particular, crystalline GaN nanowire arrays with good alignment have attracted extensive

<sup>a</sup>Shenyang National Laboratory for Materials Science (SYNL), Institute of Metal Research (IMR), Chinese Academy of Sciences (CAS), No. 72, Wenhua Road, Shenhe District, Shenyang 110016, China. E-mail: baodanliu@hotmail.com, xjiang@imr.ac.cn

<sup>b</sup>University of Chinese Academy of Sciences, 19 A Yuquan Road, Shijingshan District, Beijing, 100049, China

<sup>c</sup>CIMAP CNRS/CEA/ENSICAEN/Normandie University, 6 Bd Maréchal Juin, 14050 Caen Cedex 4, France

<sup>d</sup>Institute of High Technology Physics, National Research Tomsk Polytechnic University, 30 Lenin Ave., 634050 Tomsk, Russia

†Electronic supplementary information (ESI) available: Experimental set-up, photograph and SEM images, VLS growth model, atomic structure and line-scan elemental profiles of GaN nanowires. See DOI: 10.1039/c7nr00032d

research interest due to their strain relieving properties, enhanced sidewall emission by exposure of different facets, and increased light output and extraction efficiency. Typically, by virtue of their nanometer scale size and distinct growth mechanism,<sup>18</sup> vertically-oriented GaN nanowires accommodate strain at the growth heterointerfaces, reducing the density of threading dislocations which otherwise act as non-radiative recombination centers leading to an internal quantum efficiency decrease.<sup>19</sup>

To obtain vertically aligned GaN nanowire arrays, several synthetic strategies have been developed in the past few years. For instance, earlier studies demonstrated that vertical GaN nanowires with a confined nucleation location, diameter and orientation can be obtained using a patterned SiO<sub>2</sub> mask fabricated by interferometric lithography or with an anodic aluminum oxide (AAO) mask.<sup>20,21</sup> In this way, the GaN nanowires show uniform dimensional sizes and excellent alignment, which are accurately defined by the mask pore size and depth. However, the removal of SiO<sub>2</sub> or AAO masks is strenuous and occasionally destroys the GaN nanostructures. The molecular beam epitaxy (MBE) technology can also produce well-aligned GaN nanowires or nanorods with decent crystal quality and chemical purity on a variety of substrates through slow and precise Ga and N precursor control.<sup>22,23</sup> The GaN nucleation sites can also be well defined when a thin mask is used. For example, position-controlled growth of GaN nanowires and nanotubes can be prepared by means of MBE on a thin titanium mask structured diamond.<sup>24</sup> The Ti masks with periodic holes allow for the tuning of the diameter and interval distances of the nanowire arrays. Similar GaN nanowire array synthesis can also be achieved by metal organic chemical vapor deposition (MOCVD) and the alignment control of GaN nanowires can be easily realized on the basis of complex optimization of precursor pressure and distribution manipulations.<sup>25,26</sup> The key problem of the above-mentioned MBE and MOCVD growth of GaN nanowire arrays comes from the ultra-high vacuum and the complicated control process, which makes the aligned GaN growth more challenging. As an alternative strategy, the catalytic epitaxy of GaN nanowires on a suitable crystalline substrate has been demonstrated as feasible from the viewpoint of either theoretical or experimental studies. The close lattice constants of GaN and substrates (sapphire, SiC, ZnO, *etc.*) enable a direct epitaxy nucleation of GaN nanocrystals and their orientation can be directly governed by the initial substrate orientation. Typical examples of epitaxial GaN nanowire arrays can be found in wurtzite GaN nanowires in the orthogonal  $[1\bar{1}0]$  and  $[001]$  directions epitaxially grown on  $(100)$   $\gamma$ -LiAlO<sub>2</sub> and  $(111)$  MgO single-crystal substrates.<sup>18</sup> Among them, the sapphire substrate is most widely adopted in GaN epitaxial growth due to its close crystal structure symmetry and low production cost. Many advantageous applications can be expected from the scalable production of GaN nanowires with good alignment. For instance, the Wang group<sup>27</sup> proposed that GaN nanowire arrays are the ideal candidates for the homoepitaxial growth of high-quality GaN crystals with reduced threading dis-

location density. In addition, GaN nanowire arrays on a *c*-plane sapphire substrate also demonstrate great potential in optoelectronic applications.<sup>28,29</sup> However, the alignment uniformity of GaN nanowires on the sapphire substrate synthesized from catalytic and epitaxial routines becomes more challenging with the enlargement of substrate size, which requires urgent improvement for the building of scalable optoelectronic nanodevices.

Over the past few years, our group has made considerable efforts toward the nucleation design, crystallographic alignment control, structural defect depression and cathodoluminescence study of GaN nanowires processed by CVD methods.<sup>30–33</sup> Though single-crystalline GaN nanowire arrays grown along specific crystallographic directions have been successfully obtained with or without the assistance of metal catalysts, the realization of homogeneous GaN nanowires with superior alignment on an industrially scalable substrate still remains a challenge. Particularly, with the enlargement of the substrate size, GaN nanowires with different orientations will appear and the alignment uniformity of GaN nanowires becomes poor, which will affect the integration of GaN-based nanodevices and performance stability. As a result, it is essential and technologically important to further improve the alignment homogeneity of GaN nanowires. In this work, we demonstrate a tremendous step toward the synthesis of highly-ordered GaN nanowire arrays on a 20 × 20 mm scalable sapphire substrate. Most importantly, it was found that the crystallographic growth direction of GaN nanowire arrays is closely related to the NH<sub>3</sub> flowing rate and a low NH<sub>3</sub> flowing rate can lead to a significant improvement of GaN nanowire alignment. X-ray diffraction measurement confirms the preferential orientation of GaN nanowires along the  $[0001]$  direction and a high-resolution transmission electron microscopy (HRTEM) study on the GaN/sapphire interface suggests that the GaN crystal is directly nucleated on the sapphire surface to generate epitaxial growth. However, periodic dislocation is also observed in the GaN/sapphire interface to release the structural strain due to the lattice mismatching. A photoluminescence study on the well-aligned GaN nanowires found a sharp emission band with a maximum peak centered at 385 nm and a weak dome in the visible range. The realization of scalable GaN nanowires with good alignment paves a solid way toward the integration of GaN-based optoelectronic nanodevices such as nano-LEDs, UV-photo-detectors and self-powered nano-generators.

## Experimental section

The highly-ordered GaN nanowire arrays were fabricated *via* a simple chemical vapor deposition process, as described in our previous work.<sup>33</sup> The  $[0001]$ -orientated sapphire substrate previously coated with a 5 nm Au layer by an electron beam deposition method was used as the nucleation site of GaN nanowires.<sup>31</sup> High purity gallium oxide (Ga<sub>2</sub>O<sub>3</sub>) powders and ammonia gas were employed as the precursors for the for-

mation of GaN crystals. An alumina boat with Ga<sub>2</sub>O<sub>3</sub> powder was placed in the center of a quartz tube heated in a horizontal tube furnace (Fig. S1†). The temperature was increased to 1100 °C from room temperature to promote the decomposition of the Ga<sub>2</sub>O<sub>3</sub> powder and NH<sub>3</sub> gas at a flowing rate of 10–50 standard-state cubic centimeter per minute (sccm) was introduced into the growth chamber from the beginning of the temperature increase. The growth of GaN nanowires was maintained at 1100 °C for a certain period of time and then cooled down to room temperature under the protection of flowing Ar gas (100 sccm). The morphologies of samples were characterized by using a field-emission scanning electron microscope (FE-SEM) operating at 20 kV (SEM Zeiss, Supra 55). The phase and purity of the as-grown GaN nanowires were examined by using a Rigaku RINT 2000 X-ray powder diffractometer (XRD) with Cu K<sub>α</sub> radiation, operating at 40 kV and 40 mA. Cross-sectional transmission electron microscopy (TEM) samples were prepared in a classical way by slicing, gluing, grinding and final ion milling with a Gatan PIPS 691. In addition, a focused ion beam system (FEI Helios NanoLab 600) was also used to produce a thin foil. In the latter case, the deposition of a protective platinum strip was carried out to act as an impingement plate followed by ion milling using Ga<sup>+</sup> ions until electronic transparency was achieved. The microstructure, crystallinity and chemical composition of the samples were observed using a high-resolution TEM (FEI, Tecnai G2 F20 and JEM ARM200F cold field emission gun (FEG) probe and image aberration corrected electron microscope both operated at 200 kV) attached with an X-ray energy dispersion spectrometer

(EDS) and electron energy loss spectrometer (EELS) (Quantum ER965 from Gatan). Photoluminescence (PL) spectra were recorded at room temperature using a 325 nm He–Cd laser with 10 mW power.

## Results and discussion

To optimize the alignment control, the growth experiments of GaN nanowires are carried out at different NH<sub>3</sub> flux rates. Fig. 1 shows the representative cross-sectional SEM images and XRD patterns of GaN nanowires at different NH<sub>3</sub> flowing rates and an obvious morphology and alignment evolution as a dependence of the NH<sub>3</sub> flowing rate can be observed, suggesting that the flux of NH<sub>3</sub> gas plays a crucial role in governing the nucleation and alignment of GaN nanowires. Typically, a large NH<sub>3</sub> flowing rate of 50 sccm will result in poor alignment of GaN nanowires, as seen in Fig. 1b. In this case, the GaN nanocrystals have a fast nucleation rate on the sapphire surface to produce a particle like film and the separated nanowires cannot be obtained, as schematically illustrated in Fig. 1a. However, with the further deposition of GaN nanoparticles, some GaN nanowires with preferential orientation along the *c*-axis of wurtzite GaN can be formed, as verified by the strong peak intensity of the (0002) plane in the XRD pattern (Fig. 1d). The appearance of the (10 $\bar{1}$ 0) and (10 $\bar{1}$ 1) peaks further implies the poor alignment of GaN nanowires under a high NH<sub>3</sub> flux. In addition, the top-view SEM image (Fig. 1c) also shows the random growth of GaN nanowires, in

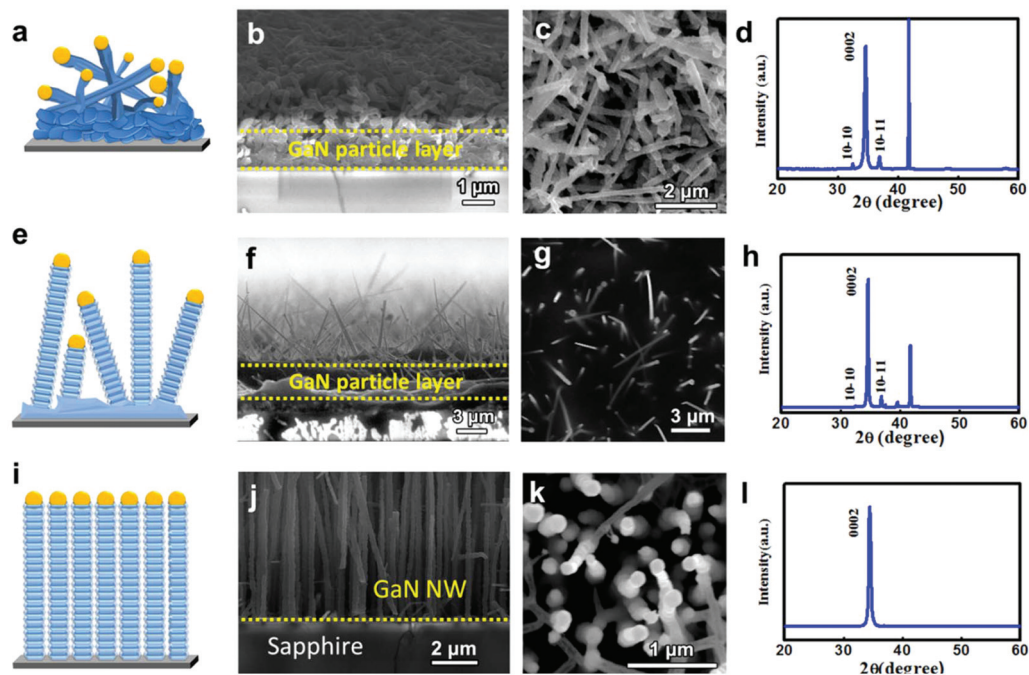


**Fig. 1** ((a–d), (e–h) and (i–l)) The schematic crystal models, cross-sectional SEM images, top-view SEM images and XRD patterns of GaN nanowires at NH<sub>3</sub> flux rates of 50 sccm, 15 sccm and 10 sccm respectively, showing the alignment evolution of three typical GaN nanowires depending on different NH<sub>3</sub> flux rates.



good agreement with the cross-section SEM result. Apparently, the formation of the GaN nanowires occurs in two continuous stages: (1) the deposition of the GaN nanoparticle layer and (2) the growth of helical GaN nanowires *via* the Au-assisted process. The decrease of the  $\text{NH}_3$  flowing rate from 50 to 15 sccm leads to a significant alignment improvement of the GaN nanowires, as shown in the cross-section and top-view SEM images (Fig. 1f and g). It seems that the GaN still prefers to form some initial nanoparticle layer and then the GaN nanowires grow on the top of this layer, as described in the schematic of Fig. 1e. Similar nucleation and growth behaviors of GaN nanostructures have been observed in our previous work.<sup>31</sup> Correspondingly, the (0002) peak still exhibits a high intensity in the XRD pattern (Fig. 1h), whereas the (10 $\bar{1}$ 0) and (10 $\bar{1}$ 1) peaks tend to disappear, further demonstrating the alignment enhancement of GaN nanowires under lower  $\text{NH}_3$  flux. When the  $\text{NH}_3$  gas flowing rate is further decreased to 10 sccm, highly-aligned GaN nanowires grown vertically on the sapphire substrate are observed, as schematically described in Fig. 1i and presented in the cross-section and top-view SEM images shown in Fig. 1j and k. Correspondingly, only the (0002) peak with a strong diffraction intensity is observed in the XRD pattern, and the (10 $\bar{1}$ 0) and (10 $\bar{1}$ 1) peaks disappear (Fig. 1l). This means that all the GaN nanowires are oriented along the [0001] direction to form uniformly aligned nanowires, and these well-aligned GaN nanowires with uniform dimensional size have been realized on a 20 × 20 mm sapphire substrate (Fig. S2†). Different from the GaN nanowires shown in Fig. 1b and f, the GaN nanowires at a  $\text{NH}_3$  flux rate of 10 sccm are directly nucleated on the substrate surface without any interlayer observed at the interface (Fig. 1j).

The direct epitaxy of GaN nanowires on the sapphire substrate at the  $\text{NH}_3$  flux rate of 10 sccm and their good alignment allow us to further investigate the nucleation and growth mechanism. Typically, these GaN nanowires exhibit corrugated morphology and gold catalytic particles are found to terminate at the tip-end, as shown in Fig. 2a. The observation of Au nanoparticle catalysts suggests that the growth of the GaN

nanowires follows the vapor–liquid–solid (VLS) process.<sup>34</sup> Ga adatoms decomposed from vaporized  $\text{Ga}_2\text{O}_3$  powder will be directly adsorbed onto the melting Au droplets to form eutectic Au–Ga melt,<sup>35</sup> which serves as the catalyst to assist the GaN nanowire growth. The diffusion and dissolution of  $\text{NH}_3$  gas into the Au–Ga melts will lead to the supersaturation of the catalytic droplets. Notably, a low  $\text{NH}_3$  flowing rate, as employed in Fig. 1j and k, will provide a relative stable gas flow field around the vicinity of the substrate surface, and thus the supersaturated catalytic droplets are in good contact with the sapphire surface. In this way, the GaN nuclei would crystallize from the supersaturated catalytic Au–Ga melts at the liquid–solid interface and maintain a favorable epitaxial relationship, which will confine the growth of GaN along the crystalline orientation of the underlying sapphire substrate and eventually evolve into nanowires with uniform alignment, as schematically described in Fig. S3.† In addition, the absence of GaN nanowires in the region without the Au catalyst further demonstrates the VLS growth process, as shown in Fig. S4.† Unlike the smooth side surface of GaN nanorods,<sup>36</sup> the GaN nanowires synthesized in this work exhibit a corrugated appearance, which is composed of periodic concave and convex crystalline planes, as clearly observed in the SEM image and TEM image (Fig. 2a–c). The same morphology has once been observed in GaN nanorods grown on a graphite substrate in our previous work<sup>37</sup> and it is assumed that the formation of such corrugated morphology can be regarded as a combined effort of both the oscillation in nanowires' radial growth<sup>38</sup> and the competing result of electrostatic interaction energy in the concave and convex planes.

Considering the crucial importance of growth temperature in nanowire synthesis, the influence of temperature on the growth of GaN nanowires is also investigated. It has been reported that the growth temperature influences the gas phase diffusion and substrate surface diffusion motilities.<sup>39</sup> The Ga adatom desorption rate on the substrate surface would be accelerated by increasing the substrate temperature, thus the nucleation process would be suppressed and the GaN nano-

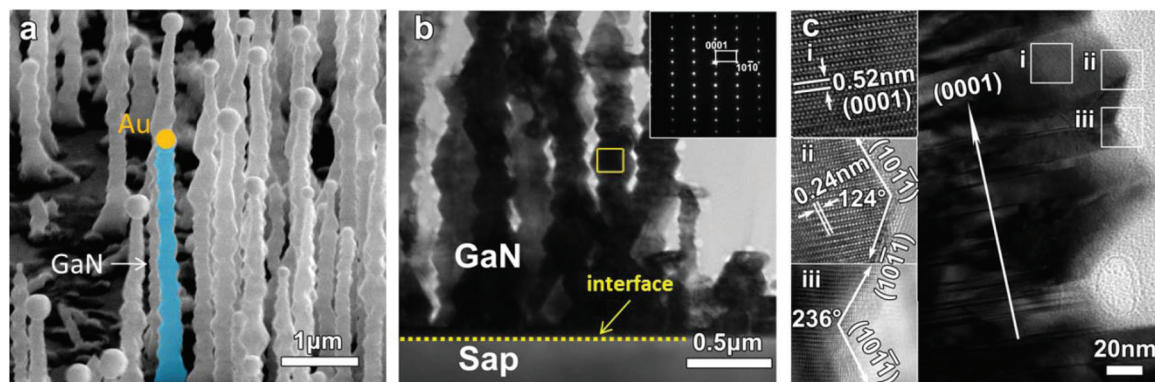


**Fig. 2** (a) Tilted SEM image and (b) low magnification cross-sectional TEM image of GaN nanowires epitaxially grown on sapphire; (inset is the corresponding SAED pattern obtained from the selected area of an individual nanowire labelled by a yellow box); (c) high-resolution TEM images of the GaN nanowires obtained from three different areas marked with i, ii and iii, respectively.

wire density reduces.<sup>40</sup> A similar tendency in nanowire density reduction has been observed when the growth temperature increases to above 1150 °C (Fig. S5†). Surprisingly, the increase of growth temperature has less impact on the alignment of the as-obtained GaN nanowire arrays. We assume the reason is the short transport distance of the reactive adatoms from the Ga<sub>2</sub>O<sub>3</sub> precursors to the substrate surface, as illustrated in Fig. S1.†

The detailed morphology and crystal structure of the vertically-aligned GaN nanowire arrays are further analyzed with the help of TEM. Fig. 2b shows the low-magnification cross-sectional TEM image and we can confirm again the vertical standing of GaN nanowires with a rough and corrugated surface. In addition, we did not find an apparent interlayer between the GaN nanowires and sapphire substrate, implying the epitaxial nucleation and growth of GaN nanowires on the sapphire substrate at a lower NH<sub>3</sub> flux rate of 10 sccm. The selective area electron diffraction (SAED) pattern obtained along the [12 $\bar{1}$ 0] zone axis of the selected area (yellow box) of the representative GaN nanowire arrays (inset in Fig. 2b) exhibits succinct diffraction spots, demonstrating their single-crystalline nature. From the corresponding high-resolution bright-field TEM image shown in Fig. 2c, one can see that the measured interplanar spacing of the lattice planes along the long-axis direction is 0.52 nm (Fig. 2c-i), corresponding to the (0001) plane and indicating the *c*-axis oriented growth of GaN nanowires. A representative protruded edge from an individual GaN nanowire is also selected to measure the side facets (Fig. 2c-ii). As can be seen, the interplanar spacing of the lattice plane parallel to the side surface is 0.24 nm, which is in good accordance with the {10 $\bar{1}$ 1} plane of GaN. The angle between the neighboring crystalline facets is roughly measured to be 124°, which is consistent with the intersection angle between {10 $\bar{1}$ 1} and {10 $\bar{1}$  $\bar{1}$ } lattice planes (Fig. S6†). Therefore, the periodic parallel side facets can be confidently identified as {10 $\bar{1}$ 1} and {10 $\bar{1}$  $\bar{1}$ } planes. The angle between the lattice planes in Fig. 2c-iii is also in agreement with this speculation.

It is assumed that the corrugated morphology is complied with the Helmholtz principle<sup>41</sup> of minimum energy dissipation, where the nanowires are enclosed by Ga<sup>3+</sup>-terminated (10 $\bar{1}$ 1) and N<sup>3-</sup>-terminated (10 $\bar{1}$  $\bar{1}$ ) polar surfaces to maintain the minimization of the energy of the system.<sup>37,42</sup> Initially, the Ga and N atoms are arranged in the *c*-plane of WZ-GaN with a favorite hexagonal shape, followed by the atoms repeatedly deposited on the previously formed GaN layer. Clearly, the deposition rate of the GaN layer along the *c*-axis direction is much faster than that on the two (10 $\bar{1}$ 1) or (10 $\bar{1}$  $\bar{1}$ ) sidewalls, leading to the formation of a one-dimensional morphology. The polar charges on the polar {10 $\bar{1}$ 1} or {10 $\bar{1}$  $\bar{1}$ } sidewalls cause electrostatic interaction energy which gradually decreases from layer to layer in a truncated hexagonal cone. When it reaches a certain point where the electrostatic surface energy makes the system unstable, opposite charged {10 $\bar{1}$  $\bar{1}$ } or {10 $\bar{1}$ 1} sidewalls are thus formed to keep the overall energy preferentially stable. In this way, the formation of corrugated GaN nanowires is finally realized through the alternation of positive and nega-

tive charges on {10 $\bar{1}$ 1} and {10 $\bar{1}$  $\bar{1}$ } sidewalls, as schematically illustrated in Fig. S3.† It is worth noting that the catalytic liquid droplet is on the nanoscale, so the size effect of the catalytic droplet is also considered.<sup>38</sup> The pressure differences in the catalytic droplet and the vapor have a significant influence on the growth kinetics. The pressure follows the Young-Laplace equation:<sup>43</sup>

$$P_{\text{in}} = P_{\text{out}} + 2\gamma_{\text{l-v}}/R$$

where  $P_{\text{in}}$  is the pressure inside the catalytic liquid droplet,  $P_{\text{out}}$  is the pressure outside the droplet,  $\gamma_{\text{(l-v)}}$  is the surface tension at the liquid-vapour interface, and  $R$  is the radius of the liquid catalytic droplet. The equation implies that when the droplet is on the nanometer scale and the growth system is under a specific pressure, the oscillation of  $R$  will lead to a strong oscillation in  $P_{\text{in}}$ . In the present VLS growth system at a temperature  $T$  and a pressure  $P_{\text{out}}$ , there should be a point where the vapor and liquid phases are in equilibrium. At this point, the chemical potential of the droplet with the equilibrium  $R_c$  must be the same as the chemical potential of the vapor. However, the actual chemical potential of the droplet would be far away from equilibrium during the growth, so the droplet would approach the equilibrium chemical potential by adjusting  $R$ . If the chemical potential of the droplet is higher than that of the vapor, the droplet will continuously evaporate, and is accompanied by a diameter increase. Eventually, the evaporation will lead to an overshoot to where the chemical potential of the droplet is lower than that of the vapor. So the droplet will absorb more vapor to increase its chemical potential. This periodic oscillation process will lead to the radius ( $r$ ) oscillation of the nanowire, which is linked with  $R$  due to the surface tension balance in the system following  $R = r \sin \theta$ , resulting in periodic oscillation in the nanowires' radial growth. Similar morphologies are commonly seen in other hexagonal structures.<sup>44</sup>

To disclose the atomic arrangement at the GaN/sapphire interface and further understand the nucleation mechanism, cross-sectional high-resolution TEM is utilized to determine the exact epitaxial relationship between the crystalline GaN nanowires and sapphire substrate. Fig. 3a shows a cross-sectional HRTEM image in the interfacial region. The atomically sharp interface between GaN and sapphire crystal domains suggests a direct epitaxial nucleation of GaN without the insertion of any buffering layer, distinctively different from the deposition process of GaN at a higher NH<sub>3</sub> flux rate. The interplanar spacing of the lattice plane orthogonal to the substrate surface is measured to be 0.276 nm, which is in accordance with the (10 $\bar{1}$ 0) plane of WZ-GaN. The corresponding lattice plane in the sapphire substrate parallel to the GaN (10 $\bar{1}$ 0) plane is (11 $\bar{2}$ 0) with an interplanar spacing value of 0.237 nm. Correspondingly, the *c*-planes in GaN and sapphire are parallel with each other and their lattice distances are in good agreement with their bulk crystals. The SAED pattern recorded at the interface marked with a white rectangular box in Fig. 3a further reflects the epitaxial relationship (Fig. 3b). According to the reciprocal lattice constants of WZ-GaN and the sapphire





stripes are clearly observed along the radial direction, two of which are marked by white arrows in Fig. 4a. It can be observed that the SFs are orthogonal to the growth direction of the nanowires, penetrating throughout the entire diameter. To further investigate the possible formation of SF, a HRTEM image of the nanowire is obtained along the  $[2\bar{1}\bar{1}0]$  zone axis to observe and distinguish the stacking sequences (Fig. 4c). The perfect stacking sequence ABABAB in the WZ-GaN structure is broken in the defective area by the alternation of the stacking sequence to ABABCBCACA. It is thus identified to be the type I SF, which involves one breach of the WZ stacking rule where the third-nearest neighbor should be the same.<sup>49</sup> Fig. 4d illustrates the formation of the type I SF in the WZ structure lattice. It is assumed that the formation of layer vacancies will directly lead to the generation of type I SFs with the lowest formation energy.<sup>50</sup> Such SFs have been often observed in wurtzite-type GaN and ZnS nanowires or nanobelts<sup>32,51</sup> and the temperature fluctuation/gradient is usually considered as the main reason for their formation.<sup>52</sup>

In the CVD synthesis process, gallium oxide powder is employed as the Ga source, which holds the possibilities of oxygen contamination in GaN nanowires. In addition, Van Nostrand *et al.* also claimed that the oxygen from the sapphire creates unintentional oxygen doping during GaN growth, raising its background electron concentration.<sup>53</sup> Therefore, it is essential to clarify the compositional purity of the as-synthesized nanowires. The quantitative analysis using EDS is performed on an individual GaN nanowire and we can only observe the predominant peaks from Ga, N and Cu (Cu signal comes from copper grids) elements (Fig. 5a). Ga and N elements have a uniform distribution inside the GaN nano-

wires, as verified by the elemental mapping and line-scan profiles (Fig. S7†). The weak O peak shoulder near the N peak in the EDS spectrum can be hardly observed. To further confirm the oxygen doping in GaN nanowires, energy filtered transmission electron microscopy (EFTEM) with much higher compositional resolution is then employed to examine the trace amount of O element from the GaN nanowires vertically grown on the sapphire substrate. Fig. 5b–d depict the typical zero-loss image of GaN nanowires on the sapphire substrate and its corresponding EFTEM micrographs of N (from the K edge peak at 401 eV) and O (from the K-edge peak at 532 eV) elements. The mapping of the N element in Fig. 5c matches well with the configuration of GaN nanowires, suggesting the uniform distribution of the N element inside the GaN nanowires. On the contrary, the mapping of the O element in Fig. 5d shows a predominant intensity in the sapphire substrate side and a very weak intensity in the GaN nanowire arrays, suggesting low contamination of oxygen in the GaN nanowire host. This is in agreement with the EDS spectrum in which the O related peak is hardly visible.

As a key III–V group nitride semiconductor, GaN has pervasive applications and technological importance in building high-performance optoelectronics due to its outstanding luminescence properties and the direct wide band-gap of 3.4 eV.<sup>54–56</sup> The evaluation of luminescence emissions of GaN nanowires is extremely crucial for their integration into optoelectronic nanodevices. Fig. 6 shows the PL spectrum of GaN nanowire arrays epitaxially grown on the sapphire substrate under the excitation of a 325 nm He–Cd laser. It can be seen that the GaN nanowires exhibit a dominant peak centered at 385 nm wavelength and a broad visible band in the scanning range from 330–700 nm. The 385 nm peak could be assigned to the near band-edge emission (NBE) and has been observed in various GaN nanostructures.<sup>57</sup> The value (41 nm) of the full width at half maximum (FWHM) is much larger than that of the GaN nanowires grown on buffering and barrier layers, which has a FWHM value of 17 nm.<sup>31</sup> The large FWHM value may originate from the structural strain and SFs due to the large lattice mismatching and further implies the degraded

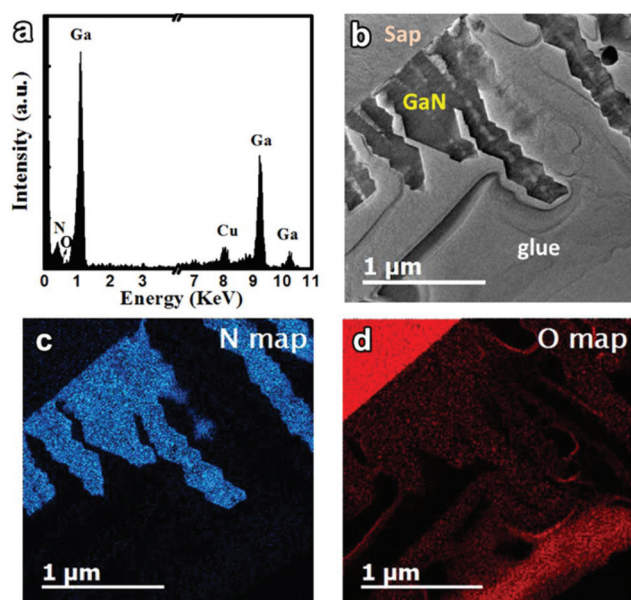


Fig. 5 (a) EDS spectrum obtained from a randomly selected individual GaN nanowire; (b) the typical zero-loss EFTEM image and its chemical mappings of (c) N (from the K edge at 401 eV) and (d) O (from the K edge at 532 eV) elements.

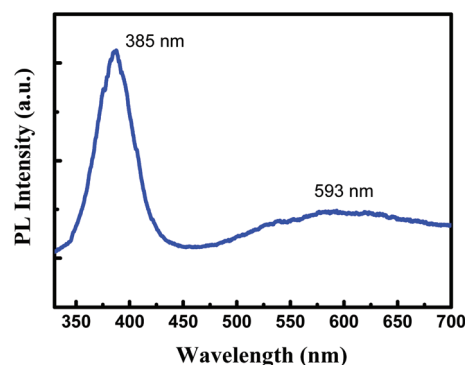


Fig. 6 Room-temperature photoluminescence spectrum of GaN nanowires epitaxially grown on a sapphire substrate under the excitation of a 325 nm He–Cd laser.



crystal quality. Occasionally, the dislocation from the underlying sapphire substrate can also be observed to thread the interface and penetrate into the GaN crystal, leading to the broadening of the NBE emission.<sup>58</sup> The weak dome peaked at 593 nm wavelength in the visible range of 500–700 nm can be assigned to the yellow luminescence (YL) emission, which is also widely observed in various GaN crystals.<sup>59,60</sup> This YL emission is widely accepted as a defect-related luminescence and is generally considered to be a key parameter to evaluate the optical performance of the GaN crystal. A higher intensity of the YL emission implies a poorer crystal quality and possible impurity contamination. Our previous work also demonstrated that the insertion of buffering and barrier layers can effectively depress the YL emission through the isolation of threading dislocations from the substrate.<sup>31</sup> In the current work, this YL band may come from the negligible oxygen contamination and the structural defects instead of threading dislocations since we did not observe these defects from TEM analysis. The luminescence properties of GaN nanowire arrays can be further improved through the homoepitaxy of GaN nanowires on the GaN substrate without lattice and thermal mismatching or the adoption of suitable buffering/barrier layers.<sup>61,62</sup> For instance, Hao and Heilmann *et al.* utilized atomically thin graphene or BN layers for the realization of high-quality GaN crystals.<sup>63,64</sup> In this way, the integration of various high-performance and high-efficiency optoelectronic nanodevices based on high-quality GaN nanowire arrays can be expected and the current work paves a solid way toward the development of GaN-based nanomaterials and nanotechnology.

## Conclusions

In summary, GaN nanowires with uniform alignment along the [0001] direction have been obtained in a simple Au-assisted CVD process. The alignment homogeneity of the GaN nanowires is further realized through the control of NH<sub>3</sub> gas at a low flowing rate. The lower NH<sub>3</sub> flowing rate enables the homogeneous nucleation of GaN on the sapphire substrate to establish the direct epitaxial relationship and the GaN growth direction can be well confined by the underlying sapphire substrate. HRTEM analysis reveals the formation of hollow cavities and the generation of stacking faults inside the GaN nanowires. Additionally, a periodic misfit dislocation is also observed to release the structural strain due to the large lattice constant mismatch between GaN and sapphire. Accurate composition analysis using EFTEM imaging finds low oxygen contamination in the GaN lattice host. Optical characterization of the GaN nanowires reveals that the nanowire arrays exhibit a sharp NBE emission band in the UV range and a weak dome in the visible range, demonstrating the decent luminescence properties of GaN nanowires. The finding in this work not only elucidates the key factor governing the alignment control of GaN nanowires on the sapphire substrate, but also further discloses the lattice matching in the GaN/sapphire interface on the atomic scale using HRTEM. Obtaining highly aligned

GaN nanowires will further promote their technologically important applications in the heteroepitaxial growth of GaN crystals, highly bright nano-LEDs, photovoltaic cells, photo-detectors and other related optoelectronic nanodevices.

## Conflict of interest

The authors declare no competing financial interest.

## Acknowledgements

This work was mainly supported by the Knowledge Innovation Program of Institute of Metal Research, Chinese Academy of Sciences with grant no. Y2NCA111A1 and Y3NCA111A1, and the Youth Innovation Promotion Association, Chinese Academy of Sciences (grant no. Y4NC711171). Xavier Portier and Christophe Labbé would like to thank Marie Pierre Chauvat for her expertise in using the FIB system for the TEM sample and also the French ANR (Agence Nationale de la Recherche) institution for the EQUIPEX “GENESIS” grant that allowed the acquisition and the use of the FIB system (HELIOS Nanolab 600 from FEI) and the EELS spectrometer (QUANTUM ER965 from GATAN).

## References

- 1 A. I. Hochbaum and P. Yang, *Chem. Rev.*, 2009, **110**, 527–546.
- 2 K. Tomioka, F. Izhizaka and T. Fukui, *Nano Lett.*, 2015, **15**, 7253–7257.
- 3 K. Nagashima, T. Yanagida, K. Oka, M. Taniguchi, T. Kawai, J.-S. Kim and B. H. Park, *Nano Lett.*, 2010, **10**, 1359–1363.
- 4 E. Garnett and P. Yang, *Nano Lett.*, 2010, **10**, 1082–1087.
- 5 S. W. Boettcher, J. M. Spurgeon, M. C. Putnam, E. L. Warren, D. B. Turner-Evans, M. D. Kelzenberg, J. R. Maiolo, H. A. Atwater and N. S. Lewis, *Science*, 2010, **327**, 185–187.
- 6 X. Zhang, Y. Liu and Z. Kang, *ACS Appl. Mater. Interfaces*, 2014, **6**, 4480–4489.
- 7 Y. Huang, X. F. Duan, Q. Q. Wei and C. M. Lieber, *Science*, 2001, **291**, 630–633.
- 8 A. V. Akimov, J. T. Muckerman and O. V. Prezhdo, *J. Am. Chem. Soc.*, 2013, **135**, 8682–8691.
- 9 B. O. Jung, S.-Y. Bae, S. Y. Kim, S. Lee, J. Y. Lee, D.-S. Lee, Y. Kato, Y. Honda and H. Amano, *Nano Energy*, 2015, **11**, 294–303.
- 10 Z. Yan, G. Liu, J. M. Khan and A. A. Balandin, *Nat. Commun.*, 2012, **3**, 827.
- 11 C.-Y. Chen, G. Zhu, Y. Hu, J.-W. Yu, J. Song, K.-Y. Cheng, L.-H. Peng, L.-J. Chou and Z. L. Wang, *ACS Nano*, 2012, **6**, 5687–5692.

- 12 Y. B. Tang, X. H. Bo, C. S. Lee, H. T. Cong, H. M. Cheng, Z. H. Chen, W. J. Zhang, I. Bello and S. T. Lee, *Adv. Funct. Mater.*, 2008, **18**, 3515–3522.
- 13 X. B. Wang, J. H. Song, F. Zhang, C. Y. He, Z. Hu and Z. L. Wang, *Adv. Mater.*, 2010, **22**, 2155–2158.
- 14 P. Deb, H. Kim, Y. Qin, R. Lahiji, M. Oliver, R. Reifengerger and T. Sands, *Nano Lett.*, 2006, **6**, 2893–2898.
- 15 R. Koester, D. Sager, W.-A. Quitsch, O. Pflingsten, A. Poloczec, S. Blumenthal, G. Keller, W. Prost, G. Bacher and F.-J. Tegude, *Nano Lett.*, 2015, **15**, 2318–2323.
- 16 T. R. Kuykendall, M. V. Altoe, D. F. Ogletree and S. Aloni, *Nano Lett.*, 2014, **14**(12), 6767–6773.
- 17 A. H. Chin, T. S. Ahn, H. Li, S. Vaddiraju, C. J. Bardeen, C. Z. Ning and M. K. Sunkara, *Nano Lett.*, 2007, **7**, 626–631.
- 18 T. Kuykendall, P. J. Pauzauskie, Y. F. Zhang, J. Goldberger, D. Sirbully, J. Denlinger and P. D. Yang, *Nat. Mater.*, 2004, **3**, 524–528.
- 19 Y. Sun, Y.-H. Cho, H.-M. Kim and T. W. Kang, *Appl. Phys. Lett.*, 2005, **87**, 093115.
- 20 S. D. Hersee, X. Sun and X. Wang, *Nano Lett.*, 2006, **6**, 1808–1811.
- 21 J. Zhang, L. D. Zhang, X. F. Wang, C. H. Liang, X. S. Peng and Y. W. Wang, *J. Chem. Phys.*, 2001, **115**, 5714–5717.
- 22 S. Fernández-Garrido, V. M. Kaganer, K. K. Sabelfeld, T. Gotschke, J. Grandal, E. Calleja, L. Geelhaar and O. Brandt, *Nano Lett.*, 2013, **13**, 3274–3280.
- 23 V. M. Kaganer, S. Fernández-Garrido, P. Dogan, K. K. Sabelfeld and O. Brandt, *Nano Lett.*, 2016, **16**(6), 3717–3725.
- 24 F. Schuster, M. Hetzl, S. Weiszer, J. A. Garrido, M. de la Mata, C. Magen, J. Arbiol and M. Stutzmann, *Nano Lett.*, 2015, **15**(3), 1773–1779.
- 25 C. G. Tu, C. Y. Su, C. H. Liao, C. Hsieh, Y. F. Yao, H. T. Chen, C. H. Lin, C. M. Weng, Y. W. Kiang and C. C. Yang, *Nanotechnology*, 2016, **27**, 025303.
- 26 P. M. Coulon, B. Alloing, V. Brandli, D. Lefebvre, S. Chenot and J. Zuniga-Perez, *Phys. Status Solidi B*, 2015, **252**, 1096–1103.
- 27 Q. M. Li, Y. Lin, J. R. Creighton, J. J. Figiel and G. T. Wang, *Adv. Mater.*, 2009, **21**, 2416–2420.
- 28 C. T. Huang, J. Song, W. F. Lee, Y. Ding, Z. Gao, Y. Hao, L. J. Chen and Z. L. Wang, *J. Am. Chem. Soc.*, 2010, **132**, 4766–4771.
- 29 Z. Wu, M. G. Hahm, Y. J. Jung and L. Menon, *J. Mater. Chem.*, 2009, **19**, 463–467.
- 30 B. D. Liu, Z. E. Wang, F. Yuan, D. Benjamin, T. Sekiguchi and X. Jiang, *RSC Adv.*, 2013, **3**, 22914–22917.
- 31 B. D. Liu, F. Yuan, B. Dierre, T. Sekiguchi, S. Zhang, Y. K. Xu and X. Jiang, *ACS Appl. Mater. Interfaces*, 2014, **6**, 14159–14166.
- 32 B. D. Liu, Y. Bando, M. S. Wang and D. Golberg, *J. Nanosci. Nanotechnol.*, 2010, **10**, 3945–3951.
- 33 B. D. Liu, Y. Bando, C. C. Tang, F. F. Xu and D. Golberg, *Appl. Phys. Lett.*, 2005, **87**, 073106.
- 34 R. S. Wagner and W. C. Ellis, *Appl. Phys. Lett.*, 1964, **4**, 89–90.
- 35 R. E. Diaz, R. Sharma, K. Jarvis, Q. Zhang and S. Mahajan, *J. Cryst. Growth*, 2012, **341**, 1–6.
- 36 B. Liu, Z. Wang, F. Yuan, D. Benjamin, T. Sekiguchi and X. Jiang, *RSC Adv.*, 2013, **3**, 22914.
- 37 F. Yuan, B. D. Liu, Z. E. Wang, B. Yang, Y. Yin, B. Dierre, T. Sekiguchi, G. F. Zhang and X. Jiang, *ACS Appl. Mater. Interfaces*, 2013, **5**, 12066–12072.
- 38 H. Wang, J. T. Wang, Z. X. Cao, W. J. Zhang, C. S. Lee, S. T. Lee and X. H. Zhang, *Nat. Commun.*, 2015, **6**, 6412.
- 39 S. Chae, K. Lee, J. Jang, D. Min, J. Kim and O. Nam, *J. Cryst. Growth*, 2015, **409**, 65–70.
- 40 S. Zhao, M. G. Kibria, Q. Wang, H. P. T. Nguyen and Z. Mi, *Nanoscale*, 2013, **5**, 5283–5287.
- 41 D. G. Christopherson and D. Dowson, *Proc. R. Soc. A*, 1959, **251**, 550–564.
- 42 X. Xie, G. Z. Wang, Z. B. Shao and D. P. Li, *J. Phys. Chem. C*, 2009, **113**, 14633–14637.
- 43 F. L. Román, J. Faro and S. Velasco, *Am. J. Phys.*, 2001, **69**, 920–921.
- 44 R. Yang, Y. Ding and Z. L. Wang, *Nano Lett.*, 2004, **4**, 1309–1312.
- 45 L. Liu and J. H. Edgar, *Mater. Sci. Eng., R*, 2002, **37**, 61–127.
- 46 D. Tham, C. Y. Nam and J. E. Fischer, *Adv. Funct. Mater.*, 2006, **16**, 1197–1202.
- 47 Y.-D. Lin, A. Chakraborty, S. Brinkley, H. C. Kuo, T. Melo, K. Fujito, J. S. Speck, S. P. DenBaars and S. Nakamura, *Appl. Phys. Lett.*, 2009, **94**, 261108.
- 48 B. D. Liu, Y. Bando, C. C. Tang, G. Z. Shen, D. Golberg and F. F. Xu, *Appl. Phys. Lett.*, 2006, **88**, 093120.
- 49 B. Yang, B. Liu, Y. Wang, H. Zhuang, Q. Liu, F. Yuan and X. Jiang, *Nanoscale*, 2015, **7**, 16237–16245.
- 50 B. D. Liu, B. Yang, B. Dierre, T. Sekiguchi and X. Jiang, *Nanoscale*, 2014, **6**, 12414–12420.
- 51 J. Lahnemann, U. Jahn, O. Brandt, T. Flissikowski, P. Dogan and H. T. Grahn, *J. Phys. D: Appl. Phys.*, 2014, **47**, 423001.
- 52 F. Meng, M. Estruga, A. Forticaux, S. A. Morin, Q. Wu, Z. Hu and S. Jin, *ACS Nano*, 2013, **7**, 11369–11378.
- 53 J. E. Van Nostrand, J. Solomon, A. Saxler, Q. H. Xie, D. C. Reynolds and D. C. Look, *J. Appl. Phys.*, 2000, **87**, 8766.
- 54 I. Akasaki, *Angew. Chem., Int. Ed.*, 2015, **54**, 7750–7763.
- 55 H. Amano, *Angew. Chem., Int. Ed.*, 2015, **54**, 7764–7769.
- 56 S. Nakamura, *Angew. Chem., Int. Ed.*, 2015, **54**, 7770–7788.
- 57 B. Liu, L. Hu, C. Tang, L. Liu, S. Li and J. Qi, *Mater. Sci. Eng., B*, 2011, **176**, 805–809.
- 58 Y. S. Chen, W. Y. Shiao, T. Y. Tang, W. M. Chang, C. H. Liao, C. H. Lin, K. C. Shen, C. C. Yang, M. C. Hsu, J. H. Yeh and T. C. Hsu, *J. Appl. Phys.*, 2009, **106**, 023521.
- 59 T. Suski, P. Perlin, H. Teisseyre, M. Leszczyński, I. Grzegory, J. Jun, M. Boćkowski, S. Porowski and T. D. Moustakas, *Appl. Phys. Lett.*, 1995, **67**, 2188–2190.

- 60 S. Xu, Y. Hao, J. Zhang, T. Jiang, L. Yang, X. Lu and Z. Lin, *Nano Lett.*, 2013, **13**, 3654–3657.
- 61 C. Wetzel, M. Zhu, J. Senawiratne, T. Detchprohm, P. D. Persans, L. Liu, E. A. Preble and D. Hanser, *J. Cryst. Growth*, 2008, **310**, 3987–3991.
- 62 H. Amano, I. Akasaki, K. Hiramatsu, N. Koide and N. Sawaki, *Thin Solid Films*, 1988, **163**, 415–420.
- 63 L. Zhang, X. Li, Y. Shao, J. Yu, Y. Wu, X. Hao, Z. Yin, Y. Dai, Y. Tian, Q. Huo, Y. Shen, Z. Hua and B. Zhang, *ACS Appl. Mater. Interfaces*, 2015, **7**, 4504–4510.
- 64 M. Heilmann, A. M. Munshi, G. Sarau, M. Goebelt, C. Tessarek, V. T. Fauske, A. T. J. van Helvoort, J. Yang, M. Latzel, B. Hoffmann, G. Conibeer, H. Weman and S. Christiansen, *Nano Lett.*, 2016, **16**, 3524–3532.